Y/DZ-2342

BWXT Y-12
A BWXT/Bechtel Enterprise

Y-12 NATIONAL SECURITY COMPLEX

MODELING OF THE MICROCHEMISTRY FOR DIFFUSION OF SELECTED IMPURITIES IN URANIUM

J. R. Kirkpatrick

Computational Modeling and Simulation Section
Computational Physics and Engineering Division
Oak Ridge National Laboratory

J. S. Bullock IV

Chemistry and Chemical Engineering Department
Technology Development Division
Y-12 National Security Complex

Issue Date: September 2001

Prepared by the
Y-12 National Security Complex
P.O. Box 2009, Oak Ridge, Tennessee 37831-8169
managed by
BWXT Y-12, LLC
for the
U.S. DEPARTMENT OF ENERGY
under contract DE-AC05-00OR22800

MANAGED BY
BWXT Y-12, L.L.C.
FOR THE UNITED STATES
DEPARTMENT OF ENERGY

UCN-13672 (10-00)

Y/DZ-2342

MODELING OF THE MICROCHEMISTRY FOR DIFFUSION OF SELECTED IMPURITIES IN URANIUM

J. R. Kirkpatrick

Computational Modeling and Simulation Section
Computational Physics and Engineering Division
Oak Ridge National Laboratory

J. S. Bullock IV

Chemistry and Chemical Engineering Department
Technology Development Division
Y-12 National Security Complex

Issue Date: September 2001

THIS PAGE INTENTIONALLY LEFT BLANK

CONTENTS

LIST OF TABLES

LIST OF FIGURES

SUMMARY

Unalloyed metallic uranium used in some work done at Y-12 contains small quantities of impurities, the three most significant of which are carbon, iron, and silicon. During metallurgical processing, as the metal cools from a molten condition towards room temperature, the metallic matrix solution becomes supersaturated in each of the impurities whose concentration exceeds the solubility limit. Many impurity atoms form compounds with uranium that precipitate out of the solution, thus creating and growing inclusions. The objective of the present work is to study the distribution of impurity atoms about some of the inclusions, with a view toward examining the effect of the interaction between inclusions on the impurity atom distribution. The method used is time-dependent mass diffusion from the supersaturated solution to the surfaces of the inclusions.

Micrographs of metal samples suggest that the inclusions form in successive stages. After each inclusion forms, it begins to draw impurity atoms from its immediate vicinity, thus altering the amounts and distributions of impurity atoms available for formation and growth of later inclusions. In the present work, a one-dimensional spherical approximation was used to simulate inclusions and their regions of influence. A first set of calculations was run to simulate the distribution of impurity atoms about the largest inclusions. Then, a second set of calculations was run to see how the loss of impurity atoms to the largest inclusions might affect the distribution of impurity atoms around the next stage of inclusions.

Plots are shown for the estimated distributions of impurity atoms in the region of influence about the inclusions for the three impurities studied. The authors believe that these distributions are qualitatively correct. However, there is enough uncertainty about precisely when inclusions nucleate and begin to grow that one should not put too much reliance on the quantitative results. This work does provide a framework and an advance toward a comprehensive model of uranium metal microchemical distributions.

THIS PAGE INTENTIONALLY LEFT BLANK

INTRODUCTION

The present work was done for Y-12 Technology Development Division. Y-12 is interested in the metallurgy of uranium and its alloys, among other reasons in order to understand the effect of microchemistry and microstructure on corrosion processes. In particular, one of the authors (JSB) is currently examining unalloyed uranium. Although there are no materials other than uranium deliberately introduced into this metal, there are nevertheless impurities that must be considered. In the present work, the authors are studying the diffusion of what are considered the three most significant of the impurities — carbon, iron, and silicon.

Micrographs of high-purity uranium metal sample surfaces[1] polished through 0.05 μm abrasive grade (see Figure 1 and Figure 2), taken with a scanning electron microscope[2] (SEM) show a distribution of inclusions formed from compounds of uranium with the many impurities. The pattern of inclusions may be explained by a process of formation of successive stages of inclusions. The largest [polygonal] inclusions seem to be left over from the previous state of the metal. That is, these are inclusions that were part of the previous solid phase and were not dissolved during the time the metal was molten. The authors refer to these as "legacy" inclusions. Between these inclusions are sets of smaller inclusions. The authors' model is that, as the resolidified metal cools, the degree of supersaturation becomes large enough that a second population of inclusions precipitates out in the spaces between the legacy inclusions. This population occupies the next largest size class of inclusions relative to the legacy inclusions. As a zeroth order approximation, one can suggest that these second stage (secondary) inclusions appear more or less simultaneously. As the metal continues to cool, successive populations of inclusions (tertiary, quaternary, etc.) precipitate in the spaces between the earlier ones. After an inclusion forms, it begins to draw impurity atoms from its immediate vicinity. This alters the amount and distribution of impurity atoms, which should have an effect on the formation and growth of later stages of inclusions.

The micrographs indicate that second and later stage inclusions are less common as one looks closer to the legacy inclusions (see Figure 1). This is consistent with the presumption that precipitation on the legacy inclusions takes impurity atoms out of the matrix so that there are fewer atoms of the impurities available to form other inclusions in the immediate vicinity of the legacy inclusions. It is also presumed that the second stage inclusions draw off impurities in their local regions of influence thus making third and later stage inclusions somewhat less common close to the second stage inclusions compared to farther away. Figure 1 and Figure 2 show regions that are almost white immediately adjacent to both legacy and second stage inclusions. These are interpreted as regions for which the larger inclusions have removed so many of the impurity atoms that there are too few impurities left to make the very small inclusions that are presumed to cause the gray color of the bulk of the micrographs. This pattern is further evidence for the belief that the larger inclusions have a significant effect on the distribution of impurity atoms and smaller inclusions in their immediate vicinity. It is of course not possible to see under the surface with this technique, so whether or not some of the closely adjacent inclusions are connected below the surface is not known.

The objective of the present work is to study the removal of impurity atoms from the immediate vicinity of inclusions by the process of diffusion to the surface of the inclusions. The authors refer to the distribution of impurity atoms in the vicinity of an inclusion as the "microchemistry". The product of the present study is an estimate of the microchemistry and some thoughts for what variables would influence it. In the time available, the authors were able to study diffusion to and precipitation on the legacy inclusions, and also into the inclusions that formed in the second stage. The impurities studied were carbon, iron, and silicon.

CALCULATIONAL MODEL

The diffusion of impurities into inclusions is a three-dimensional process. This is because the inclusions, especially the legacy inclusions, are somewhat irregular, polygonal solids (see Figure 1). Time-dependent, three- dimensional diffusion calculations are likely to be quite expensive. However, as a zeroth order approximation, one can simulate the process as one-dimensional and spherically symmetric. This is a much cheaper calculation. Of course, the further from the surface of the inclusion one gets, the less is the error in the spherical approximation. Use of a spherical approximation in the study of precipitation in solids is not unique to the present authors. It is described in Shewmon's text [3]. From footnotes and references in Shewmon, one may see that the idea was already current by the early 1960's.

The mass diffusion calculations were done using the HEATING code, version 7.2 [4]. This is a time-dependent, multidimensional heat transfer code written and maintained at ORNL. As thermal diffusion is mathematically the same as mass diffusion, the use of a heat transfer code to simulate mass diffusion is straightforward.

In a report by Taylor and Mackiewicz-Ludtka [5] it was calculated that it took roughly 400 s for the temperature in a sample uranium casting mold to drop the 100°C from solidification at 1132°C to 1032°C. Newton's Law of cooling, which is a solution for cooling of a solid body assuming a constant film coefficient, should form a reasonably satisfactory basis for estimating the curve of temperature vs time for a mold cooled by forced convection. The differential equation for temperature T vs time t for this approximation is as follows:

$$\frac{dT}{dt} = a(T - T_a)$$

where a is a constant and T_a is the ambient temperature. The solution to this differential equation is as follows:

$$(T - T_a) = (T_0 - T_a)e^{-at}$$

where T_0 is the temperature at time zero, in this case 1132°C. With T_a set to 25°C and specifying a drop from 1132°C to 1032°C in 400 s, the equation for temperature vs time becomes

$$T = 25 + 1107\exp(-2.37x10^{-4}\,t) \qquad (°C)$$

Using numerous resources [6], one of the authors (JSB) developed expressions for the diffusivity and solubility of the three different impurities as functions of temperature and of the phase of uranium existing at that temperature. Through use of a spreadsheet, these were converted into tables of diffusivity and solubility vs time which were then input into HEATING.

Solubility data found in Refs. 6a-c, for various solutes in uranium metal as the solvent, were fit to Arrhenius-type equations of the form:

$$X = \exp(a + b/T)$$

where X = atomic fraction of the solute, a and b are fitting parameters and T is temperature in Kelvins. The data for each uranium phase (α, β, and γ) was fit separately, and in the case of silicon, there was a region in the γ phase with solubility invariant with temperature. The solubility parameters used are listed in Table 1. The literature data for C and Si only gave single values for solubility in α-U, so α-phase fitting parameters

were developed that used the β-phase activation energy (*b* term) and forced the solubility at the α-β transition temperature to be equal to the value quoted in the literature (these parameters are italicized in the table). The alpha-phase solubility for each species at 600°C is also listed.

Table 1 – Parameters for Equations Describing Solubility of Species in Uranium

Solute Species	**Uranium Phase**	***a***	***b***	$X^{600°C}$
C	gamma	-2.3241	-4921.343	-----
	beta	11.5977	-19452.003	-----
	alpha	*10.5399*	*-19452.003*	8.0×10^{-6}
Si	gamma (927.5 to 985°C)	ln(0.017)	-----	-----
	gamma (790 to 927.5°C)	2.5543	-7929.914	-----
	beta	2.7522	-7627.747	-----
	alpha	*1.5850*	*-7627.747*	7.85×10^{-4}
Fe	gamma	10.3466	-16016.947	-----
	beta	6.2656	-12215.035	-----
	alpha	3.0298	-10646.674	1.049×10^{-4}

Diffusivity parameters are tabulated in Ref. 6d for a wide variety of diffusing species and solvents. These parameters are used in the equation:

$$D(T) = D_o * \exp(-Q/(R*T))$$

where $D(T)$ is the diffusivity at temperature T in Kelvins, D_o is the frequency factor, Q is the energy of activation for diffusion, and R is the universal gas constant in the same units as Q. The diffusivity parameters used are listed in Table 2.

Unfortunately, several of the species-solvent combinations needed here are not included in Ref. 6d and therefore we resorted to estimation of these parameters from examining the behavior of comparable species. This was especially useful in the estimation of phase-to-phase differences. In the case of Si, there was no comparable data available at this writing, so we used parameters characteristic of Si diffusion in aluminum (Ref. 6e) to represent the behavior in gamma-U and used estimation as mentioned to correct to the alpha and beta phase values. In the case of C, the values for several solvent species were used in a 3-D curve-fitting exercise to estimate values for C in U. This used atomic radius of the solvent species and ΔG_f of the respective carbide to arrive at values for D_o and Q. In the case of Fe, the gamma-phase data did exist, and by using diffusion data for cobalt it was possible to project values for Fe with reasonable confidence. All estimated values are italicized in the table. The resulting estimate of the diffusivity in the alpha phase at 600°C is also listed.

Table 2 – Parameters for Equations Describing Diffusivity of Species in Uranium

Diffusing Species	Uranium Phase	D_o (cm^2/s)	Q (kcal/mole)	$D^{600^\circ C}$
C	alpha	*0.07*	*30*	2.167×10^{-9}
	beta	*0.05*	*30*	-----
	gamma	*0.5*	*25*	-----
Si	alpha	*0.6*	*39*	1.038×10^{-10}
	beta	*0.583*	*43*	-----
	gamma	*0.01*	*27.725*	-----
Fe	alpha	1.15×10^{-2}	*22.7*	2.420×10^{-8}
	beta	1.15×10^{-2}	*26.9*	-----
	gamma	2.69×10^{-4}	12.0	-----

It is judged that the solubility and diffusivity estimates obtained from these parameters are adequately realistic to allow illustration of the general relative behavior in the uranium metal system.

The initial concentrations in atom fraction of the three impurities studied were as follows:

C: 0.00649

Fe: 0.0007354

Si: 0.0050134

These values represent a particular sample of "dirty" uranium (material with a rather high impurity content). The impurity levels for the material used for the micrographs could be as low as 10% of these.

By eyeball from micrograph BR 964 (Figure 1), one can simulate the legacy inclusion as being equivalent to a cube 6 microns on a side. A sphere of equivalent volume has a radius of

$$r_{legacy} = 3.7 \times 10^{-6} \text{ m}$$

From the same viewgraph, one may count 110 second stage inclusions (this is an approximate number as it is not easy to decide exactly which are second stage inclusions). The field of view is approximately 60 microns by 42 microns. This gives an average area per second stage inclusion of 22.9 micron^2/inclusion, which corresponds to a circle of radius

$$r_{outer\ second\ stage\ region\ of\ influence} = 2.7 \times 10^{-6} \text{ m}$$

In this case, the radius of the region of influence is equivalent to half the average distance between the second stage legacy inclusions.

Micrograph BR 960 (Figure 2) shows four second stage inclusions. After considerable work with a scale, one of the authors (JRK) estimated that the average radius needed to produce spherical equivalents is 468 nm. In principle, it would be best if the diffusion simulation calculation showed the inclusion growing and thus its surface area rising. The authors have not been able to work out a simple, cheap approximation for that in

HEATING. Instead, they have arbitrarily decided to use a radius that produces half the volume of a second stage inclusion. By accident, a factor of 10*sqrt(2) was lost in the calculation of the inner radius of the calculation region. By the time this error was discovered, too little time was left for calculations to be repeated with the larger second stage inner (inclusion surface) radius. Therefore, the inner radius used is 0.07 times that which corresponds to half the inclusion. Potentially, since the surface area is 5×10^{-3} times that intended, the total mass transferred to the surface could be different by a factor on that order. On the other hand, it is not clear that, considering all the other approximations in this work, the error is very great. In particular, it is not clear whether a more correct calculation of mass uptake would be done using the radius that corresponds to half the volume rather than the much smaller value. The value used in the computer calculation for the outer radius of the second stage inclusions (which is therefore the inner radius of the region to be calculated) is

$$r_{inner\ second\ stage} = 2.69 \times 10^{-8}\ \text{m}$$

The method used to do each of the calculations requires some further explanation. For the legacy inclusions, a computer case was set up using the specified legacy inclusion radius (3.7×10^{-6} m) as the inner boundary of the calculational region. A table of solubility vs time was used to specify the concentration at the inner boundary. A table of diffusivity vs time was used to specify the diffusivity for the entire volume. The initial impurity concentration was that given earlier in this section. Cases were run from zero time, which corresponded to solid metal at the melt temperature (1132°C) until a time of 2763.9 s, which represented a temperature of 600°C. By this time and temperature, it was believed that the diffusion would be slow enough that no relatively significant further transport should happen over any reasonable time scale. The boundary condition at the outer boundary was zero flux, which is equivalent to a symmetry condition. That corresponds to an assumption that the metal is composed of a series of spherical domains touching one another. For determining the outer boundary, cases were run on carbon, which has the highest diffusivity of the three impurities, with the outer radius of the calculational region increasing until the carbon concentration at the outer radius at the end of the calculation (2763.9 s) was within 0.25% of the initial value. The value used for the outer radius of the computational domain for the legacy inclusion is

$$r_{outer\ legacy\ region\ of\ influence} = 2.058 \times 10^{-3}\ \text{m}$$

The authors suspect that legacy inclusions, even in high-purity uranium such as was used for the micrographs, are much more common than are indicated by a spacing of ~2 mm (one would expect a much higher population of legacy inclusions in material with the usual impurity levels which can have on the order of ten times the impurity level of high-purity material such as that used for the micrographs). However, the curve of carbon mole fraction vs distance is so flat that there would be very little difference in the results of the calculations reported in the present document for any radius larger than a couple of hundred microns. The reader should note that, in the absence of any estimate for the spacing of legacy inclusions, the outer radius of the region of influence for the legacy inclusions is a value large enough that the influence of the legacy inclusion on the impurity levels at this radius is small. This is a somewhat different definition than that for the second stage inclusions (and any later stage inclusions) for which the region of influence is limited by the spacing between inclusions.

For the second stage inclusions, the method for calculation was substantially the same as for legacy inclusions with the addition of a bulk mass sink, and with initial conditions and the time for the case to run determined from the calculation of the legacy inclusion. The diffusion for the second stage inclusions was simulated as a linear sum of the diffusion to the legacy inclusion and to the second stage inclusion. The diffusion to the legacy inclusion was simulated as a bulk mass sink, which is a function of both time and the distance from the center of the legacy inclusion (as well of course as the identity of the impurity). At the time that represents

the beginning of significant precipitation of impurities onto the second stage inclusion, the bulk sink provides a value of the impurity concentration at the distance of the center of the second stage inclusion from the center of the legacy inclusion. This value is that due to the starting value as depleted by diffusion into the legacy inclusion. This concentration value was used as the initial condition for the entire volume about the second stage inclusion for diffusion into the second stage inclusion. For the duration of the calculation of the growth of the second stage inclusion, a time-dependent bulk sink term, which represented the values for the temporally and spatially dependent sink at the location of the center of the second stage inclusion was specified for the entire volume surrounding the second level inclusion. Of course, assuming a spatially uniform initial concentration and a spatially uniform bulk sink for the entire width of the legacy inclusion region of influence represents yet another approximation. However, the approximation is necessary in order to do a spherically symmetric calculation of the second stage inclusion.

One of the most important inputs for the second stage inclusion is the time at which the inclusion begins growing. This is a very difficult quantity to estimate. The authors developed an algorithm which they will describe, but make no claims as to its accuracy. First, it was estimated that carbon was most likely to begin precipitating first. The justification for this is that, if one examines the curves of solubility vs time for the three impurities and calculates when the solubility drops below the initial bulk impurity content, carbon reaches this level at 57.57 s whereas iron waits until 2246.57 s and silicon waits until 2248.80 s. It was further assumed that the other impurities would precipitate on the uranium carbide inclusions. For the second stage inclusions of radius 468 nm, a calculation was done to estimate the amounts of carbon, iron, and silicon in the inclusion. The calculation was done based on an assumption that the ratios of the contents of the three impurities in the inclusion were the same as the ratios of their initial concentrations in the bulk material. This is a very arbitrary assumption, but the authors were not able to come up with a better one. It would be true for the mean of all inclusion stages, although not necessarily true for a specific stage. However, it is a starting point for iteration. The assumption did allow a calculation of the contents of the impurities in the second stage inclusion, most particularly that of carbon. A particular distance from the center of the legacy inclusion was chosen for reference. This was 3.35×10^{-5} m (approximately equal to the field of view of Fig. 1), a value for which the carbon concentration at 2763.9 s in the calculation of diffusion into the legacy inclusion was 90% of the initial value. The choice of 90% for this was arbitrary. From a theoretical point of view, it might have been more reasonable to have chosen a distance infinitely far from the legacy inclusion. In any case, calculations were run iterating on the start time for the second stage inclusion until a time was found such that the amount of carbon taken by the second stage inclusion between that time and the end (2763.9 s) matched the value estimated for the content of carbon in the second stage inclusion. This time was

$$t_{start\ second\ stage\ \ incxlusion} = 2603.6 \text{ s}$$

Once this start time was determined, it was a simple matter to set up and run second stage inclusion calculations for all three of the impurities. In addition to the 33.5 microns distance, calculations were done for 16.8 microns, which is located approximately half the distance back to the surface of the legacy inclusion, 67 microns, which is approximately twice the distance from the surface of the legacy inclusion, and 2.05 mm, which is more or less infinite. For silicon, which has lower diffusivities than the other two impurities, one additional case at a distance of 8 microns was run. The bulk silicon concentration at start time at this distance is approximately 90% of the initial silicon concentration.

All the second stage cases were started at the same time regardless of the distance from the legacy inclusion. This is probably incorrect. It is likely that the inclusions farthest from the legacy inclusion will precipitate first because there is a higher carbon concentration out there and therefore the level of supersaturation at the time the second stage inclusion precipitates is higher. The authors tentatively proposed that the time for appearance of the second stage inclusion at each distance might be that for which the difference between the bulk carbon concentration and the solubility of carbon was the same as that given by the baseline results at

33.5 microns. This concept would have worked satisfactorily for the larger radii and would have led to earlier start times and therefore longer times to add mass to the inclusion. However, it was found that, for a distance of 33.4 microns, i.e., a distance only 0.1 microns inward from the baseline location, there was no value of time (less than 2763.9 s) such that the condition was satisfied. The fairly small decrease in initial concentration for the legacy inclusion and the small increase in bulk sink rate, both of course due to diffusion into the legacy inclusion, were enough that the second stage inclusion was not able to consume its desired amount of carbon. On that basis, there should not be any second stage inclusions closer to the legacy inclusion than that. This is not a reasonable result as micrographs (see Figure 1) show second stage inclusions as close as 10 microns from the center of the legacy inclusion. As a consequence, pending creation of a better way of estimating nucleation time, the authors decided to use the constant start time for second stage inclusions.

A time of 2603.6 s, which is when the calculations for second stage inclusions start, represents a temperature of 622.3°C. As was noted earlier, the calculations were stopped at 2763.9 s, which represents a temperature of 600°C. The authors suspect that the second stage inclusions will in reality start growing at much higher temperatures than 622.3°C. Also, examination of the diffusivities in the range from 2500 s to 3000 s suggests that second stage inclusion calculations will likely continue to consume noticeable amounts of the impurity materials (at least amounts that are noticeable compared to those consumed from 2603.6 s to 2763.9 s). It would be more accurate to run all the cases, both legacy and second stage inclusions, to a time corresponding to a temperature of 300°C (5876.1 s). At this temperature, the diffusivities of all three of the impurities are down at least a factor of 10^{-4} from their values at 600°C.

As lower temperatures are reached with lower D values, one can expect diffusion to be active over shorter distances, resulting in inclusion growth on even smaller scales. This would naturally lead to tertiary, quaternary and further stages of inclusion size.

CALCULATIONAL RESULTS

Plots of results from carbon calculations are shown in Figs. 3 and 4. As is noted in the captions, the x-axis (radius) is the distance from the center of the legacy inclusion. As is also noted in the caption for Fig. 4, the logarithmic scale for the x-axis (radius) makes the widths of the four second stage inclusion calculations look different whereas they in fact all have the same width. The curves with many different colors represent the results from the calculation of diffusion to the legacy inclusion. The three (four for Fig. 4) sharply cusped green curves represent calculations of the diffusion into the second stage inclusions. As one can see, the loss of carbon into the second stage inclusions within their regions of influence is substantial (for example, the maximum concentration for the 67 micron case is ~83% of the value from the legacy calculation at that radius). Put another way, the diffusion to the second stage inclusion robs carbon from the surrounding region and reduces the regional concentration relative to that which would exist if only diffusion to the legacy inclusion were operative.

Plots of results from iron calculations are shown in Figs 5 and 6. The curves with many different colors represent the results from the calculation of the legacy inclusion. The three (four for Fig. 6) sharply cusped purple curves represent calculations of the diffusion into the second stage inclusions. The loss of iron into the second stage inclusions within their regions of influence is substantial and is even higher (at least as a fraction of the amount initially available) than for carbon. For example, the maximum concentration for the 67 micron case is only ~28% of the value from the legacy calculation at that radius.

Plots of results from silicon calculations are shown in Figs. 7 and 8. The curves with many different colors represent the results from the calculation of diffusion to the legacy inclusion. The four (five for Fig. 8) sharply cusped purple curves represent calculations of the diffusion into the second stage inclusions. The loss of silicon into the second stage inclusions within their regions of influence is rather slight. For example, the maximum concentration for all but the 8 micron case is ~99.5% of the value from the legacy calculation at those radii. Even for the 8 micron case, the maximum concentration is ~97% of the value from the legacy calculation at that radius.

In an earlier section, it was shown that a good argument can be made for running cases to a later time. Also, a weak argument (weak in the sense that it is based on gut feeling rather than on calculations) was made for starting the calculations for second stage inclusion cases at earlier times than indicated in the present work. The result of running cases for second stage inclusions to a longer time would be that the boundary levels for the impurities would be even lower than shown in the figures and also the bottoms of the “holes” would be deeper. While these would represent quantitative differences, the qualitative behavior of the curves of concentration vs distance would be unchanged.

CONCLUSIONS

In principle, one might use the plots of the results of these calculations to describe the microchemistry around legacy inclusions. There is however a caveat, which is that the authors do not consider the method used for determining the time for starting the growth of second stage inclusions to be very accurate. Thus, the quantitative values for the final impurity concentrations near the second stage inclusions is in some doubt. The microchemistry given the assumptions of this simulation would consist of a pattern of quite narrow holes in a relatively smooth distribution of impurity concentration. The size (i.e., the radius) of the holes is largest for carbon and smallest for iron. As can be seen, the second stage inclusions for iron dominate the microchemistry for iron. One might expect that third stage inclusions would be poor in iron compared to the other impurities. On the other hand, the influence of the second stage inclusions for silicon is slight except of course very close to the second stage inclusions. One might expect that third stage inclusions would be relatively rich in silicon.

More accurate ways of estimating start (nucleation) times as a function of position need to be developed. Ways to incorporate position-dependent initial concentration for second stage inclusion precipitation need to be developed. Follow-on calculations, to correct certain known quantitative errors in the current calculations, will be performed. There should also be complementary SEM examination of uranium materials with higher impurity contents as a check on predictions from the calculations. As this type of analysis is continued, extension beyond melt-to-ingot cooling toward addition of heat-treatments during subsequent metallurgical processing should be an object of development.

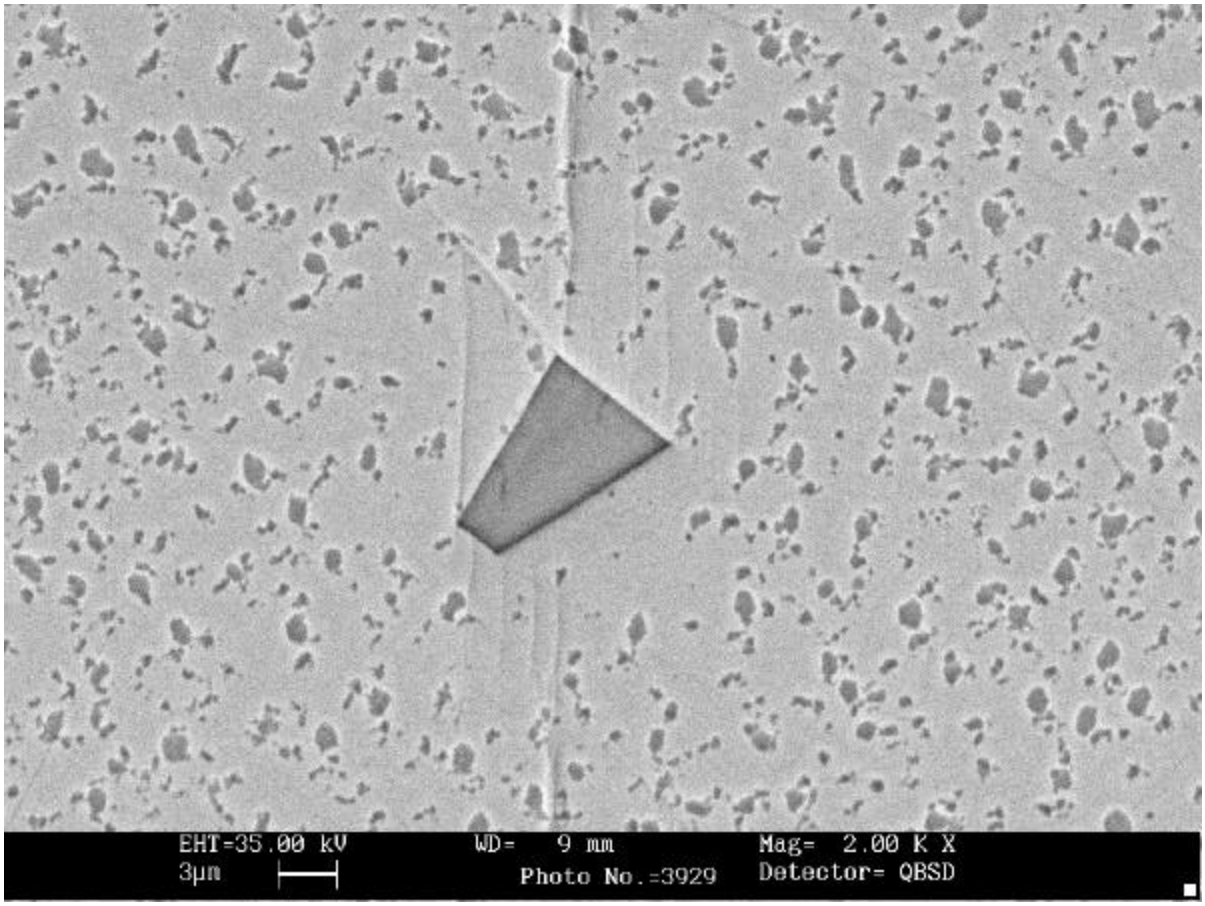

Figure 1. Micrograph BR 964 showing Legacy Inclusion and Field of Second and Third Stage Inclusions.

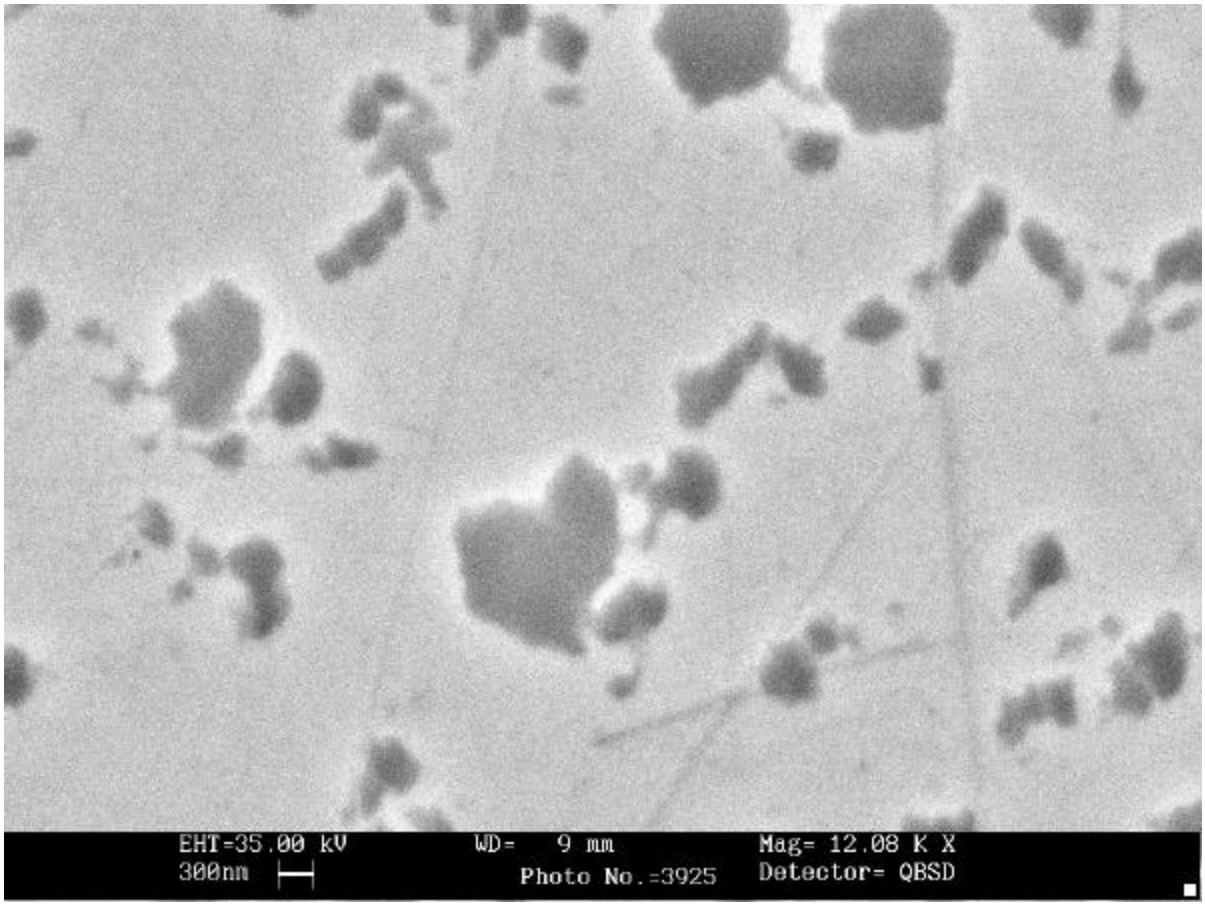

Figure 2. Micrograph BR 960 showing Four Second Stage Inclusions and Surrounding Third and Higher Stage Inclusions.

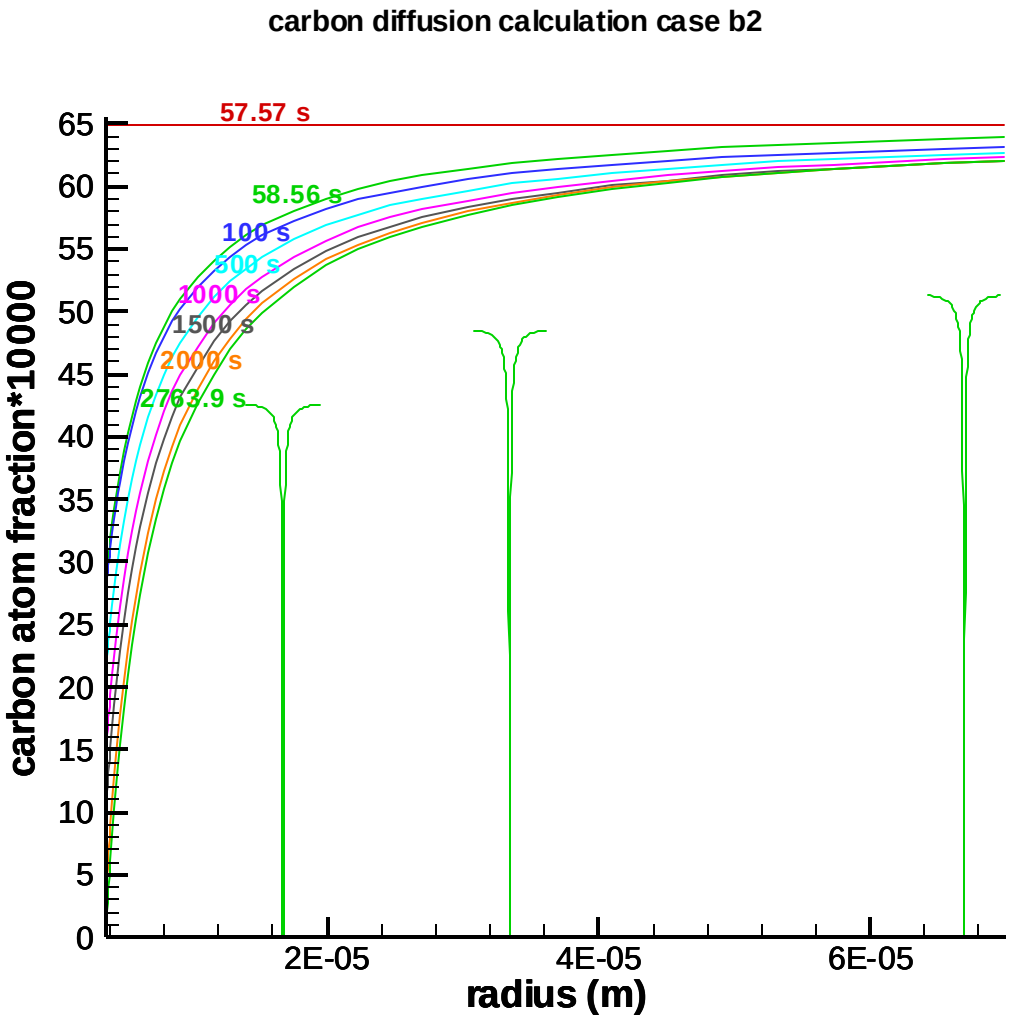

Figure 3. Plot of Carbon Atom Fraction x10^4 vs Distance from Center of Legacy Inclusion. Plot shows distribution from legacy inclusion and also distribution around second stage inclusions at three different distances.

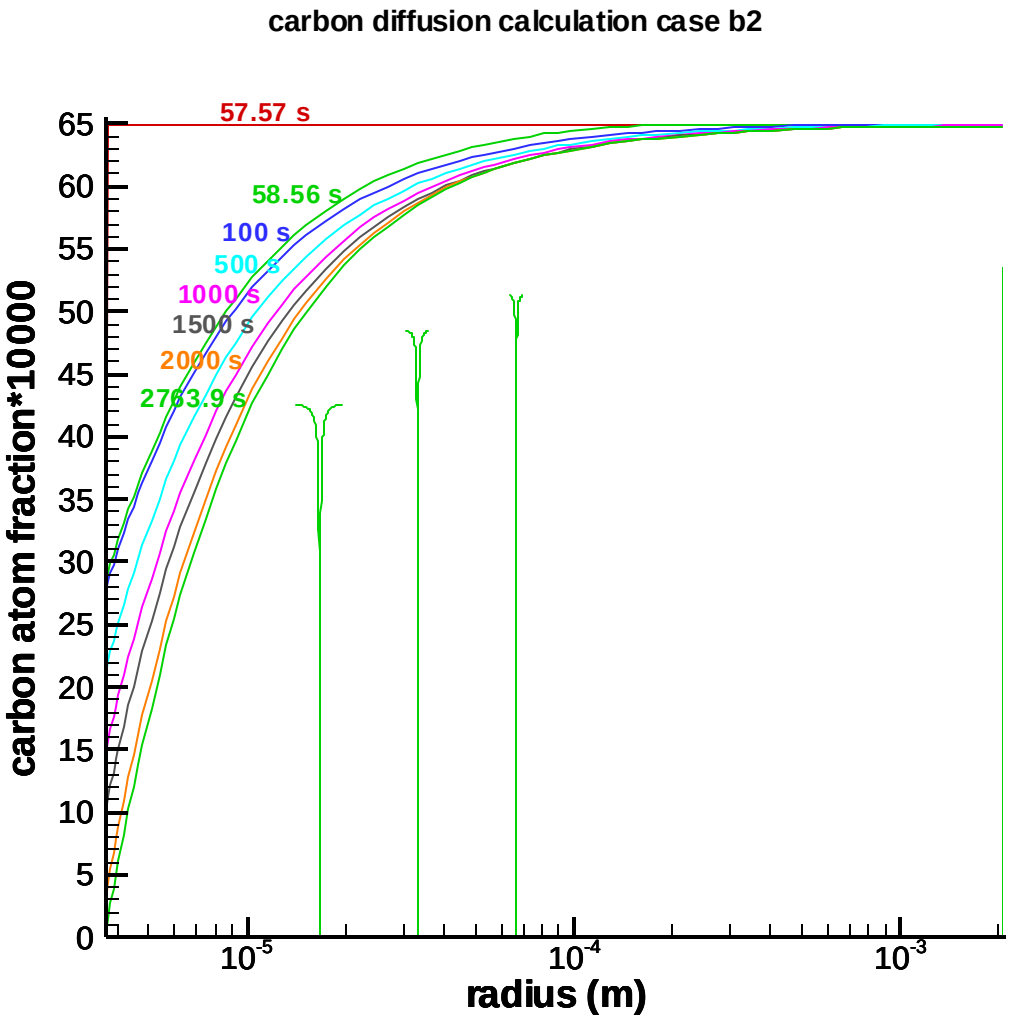

Figure 4. Plot of Carbon Atom Fraction x10^4 vs Distance from Center of Legacy Inclusion. Plot shows distribution from legacy inclusion and also distribution around second stage inclusions at four different distances. Note that the distance scale (x-axis) is logarithmic, which explains why the width of the calculational domains surrounding the second stage inclusions, which is actually the same for all the second stage inclusions, does not appear to be so on this plot.

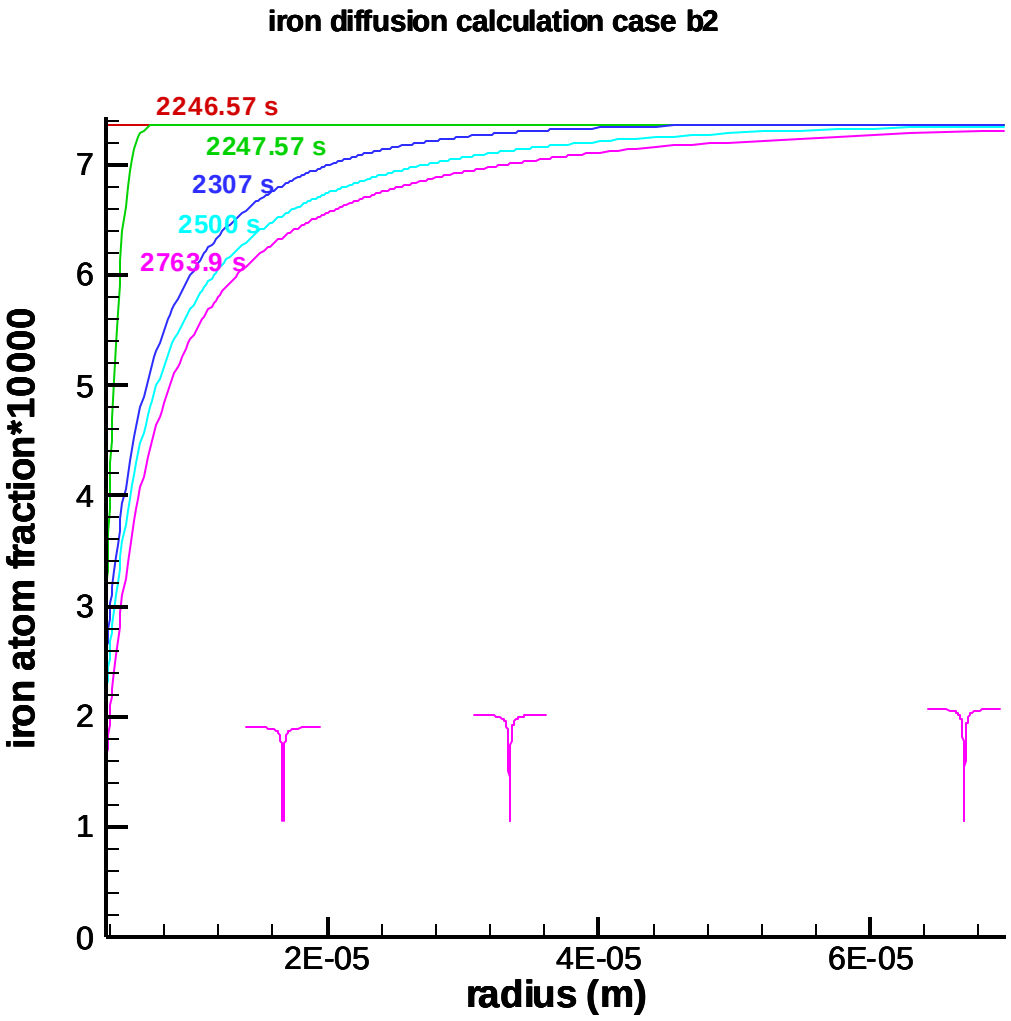

Figure 5. Plot of Iron Atom Fraction x10^4 vs Distance from Center of Legacy Inclusion. Plot shows distribution from legacy inclusion and also distribution around second stage inclusions at three different distances.

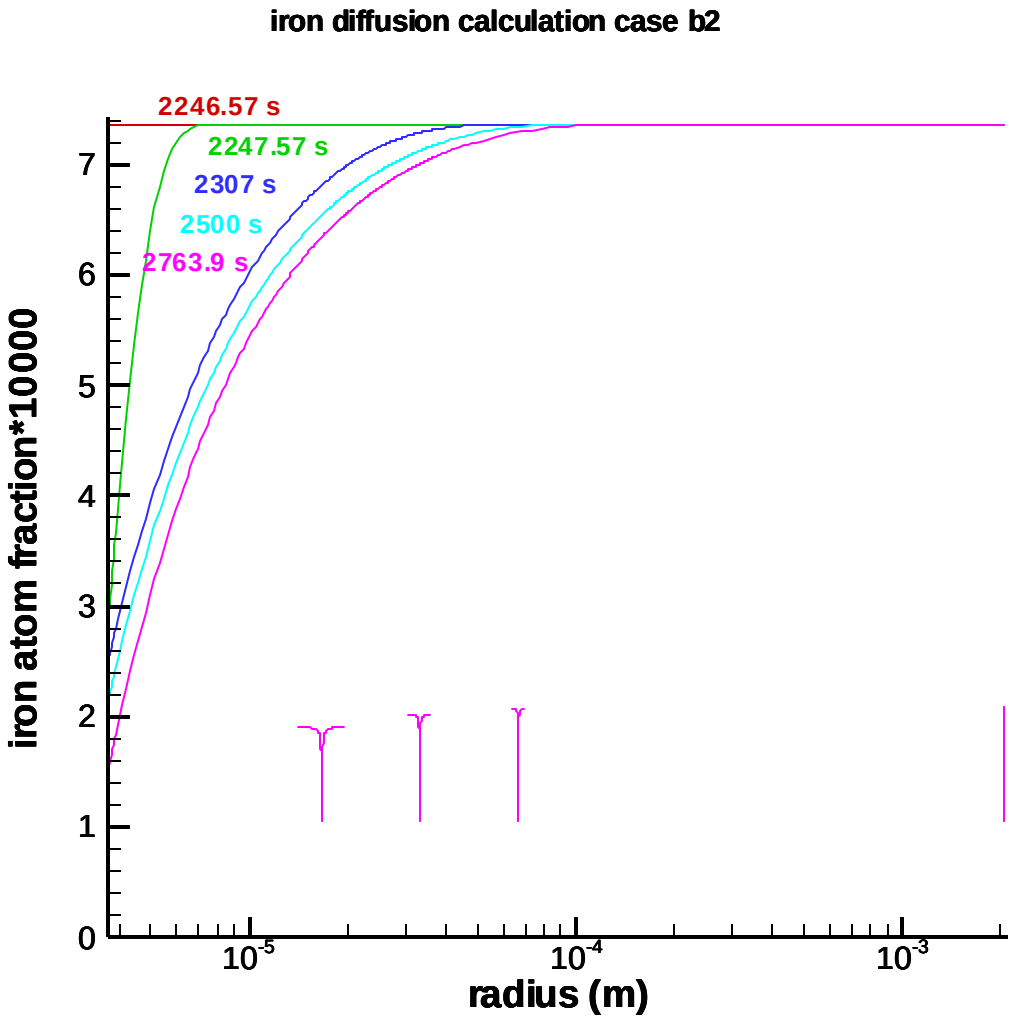

Figure 6. Plot of Iron Atom Fraction x10^4 vs Distance from Center of Legacy Inclusion. Plot shows distribution from legacy inclusion and also distribution around second stage inclusions at four different distances. Note that the distance scale (x-axis) is logarithmic, which explains why the width of the calculational domains surrounding the second stage inclusions, which is actually the same for all the second stage inclusions, does not appear to be so on this plot.

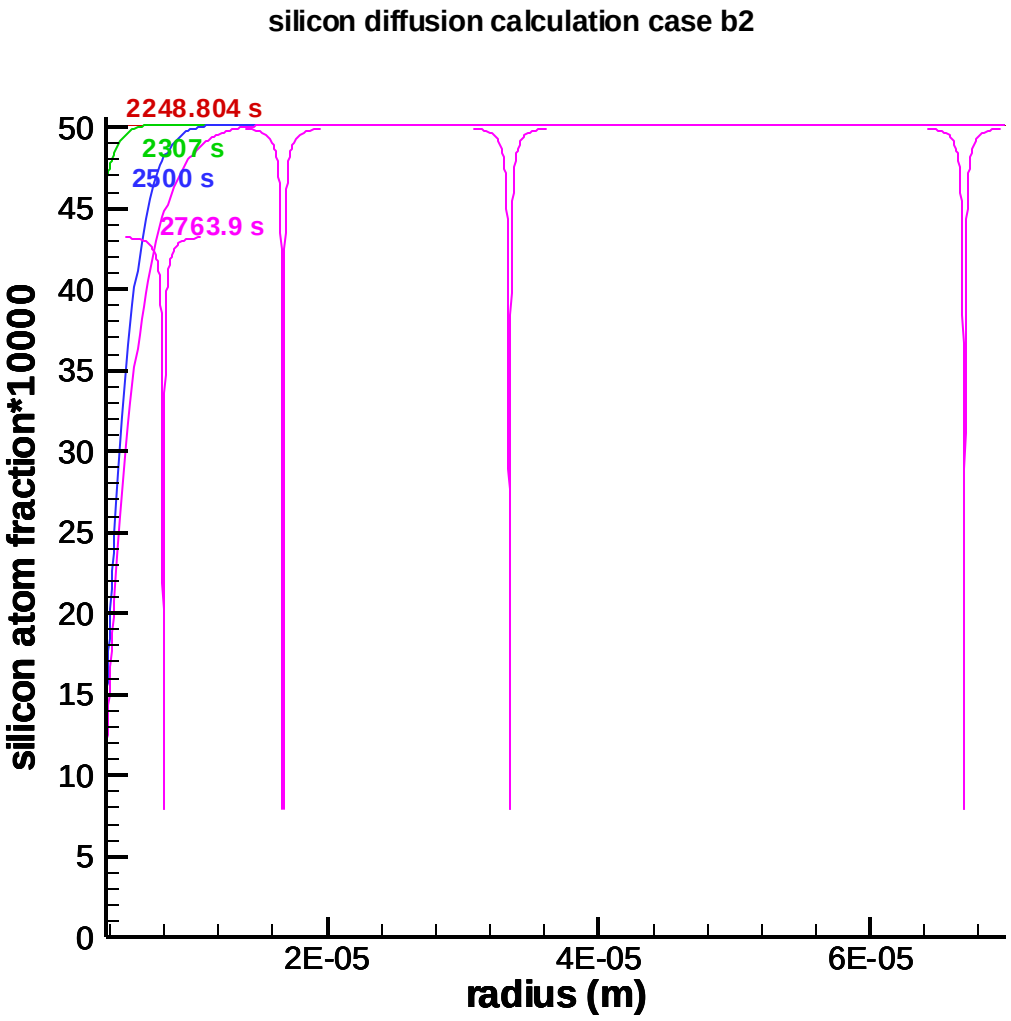

Figure 7. Plot of Silicon Atom Fraction x10^4 vs Distance from Center of Legacy Inclusion. Plot shows distribution from legacy inclusion and also distribution around second stage inclusions at four different distances.

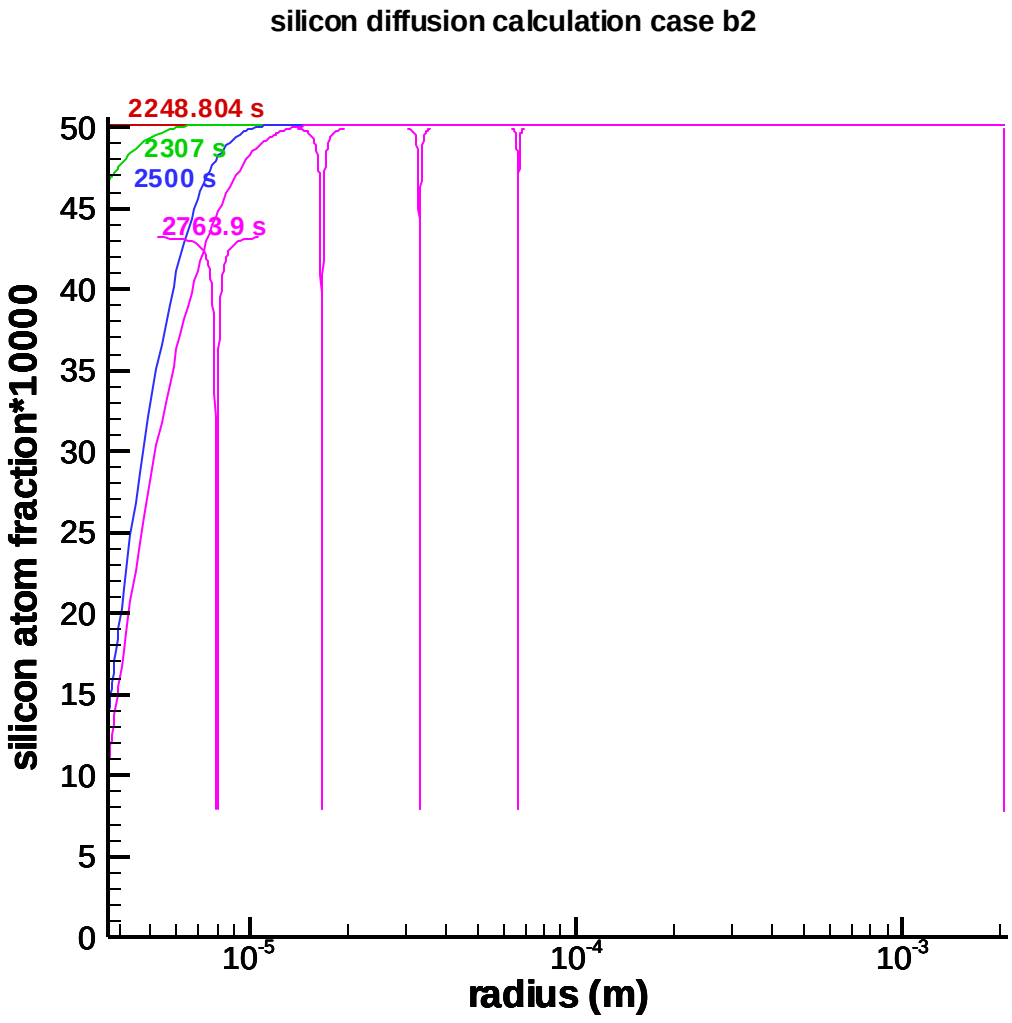

Figure 8. Plot of Silicon Atom Fraction $x10^4$ vs Distance from Center of Legacy Inclusion. Plot shows distribution from legacy inclusion and also distribution around second stage inclusions at five different distances. Note that the distance scale (x-axis) is logarithmic, which explains why the width of the calculational domains surrounding the second stage inclusions, which is actually the same for all the second stage inclusions, does not appear to be so on this plot.

REFERENCES

[1] Material provided by R. L. Bridges, Technology Development Organization, BWXT Y-12 LLC.

[2] SEM images provided by D. A. Carpenter, Technology Development Organization, BWXT Y-12 LLC.

[3] Shewmon, P., *Diffusion in Solids*, McGraw-Hill, New York, 1963.

[4] Childs, K. W., *HEATING 7.2 User's Manual*, ORNL/TM-12262, Oak Ridge National Laboratory, Oak Ridge, TN, February 1993.

[5] Taylor, M. J., and G. Mackiewicz-Ludtka, *Definition of Prominent Thermal Mechanisms Associated with the Buoyancy-Induced Transport of Hafnium-Carbide Within a Solidifying Uranium-Hafnium Alloy*, K/CSD/TM-100, Oak Ridge National Laboratory, Oak Ridge, TN, December 1992.

[6] a) Hansen, M. and K. Anderko, *Constitution of Binary Alloys, 2nd Ed*., McGraw-Hill, 1958.
b) Elliot, R. P., *Constitution of Binary Alloys, First Supplement*, McGraw-Hill, 1965.
c) Shunk, F. A., *Constitution of Binary Alloys, Second Supplement*, McGraw-Hill, 1969.
d) *Handbook of Chemistry and Physics, 70th Ed*., pp. F-54-59; CRC Press, 1990.
e) Mondolfo, L. F., *Aluminum Alloys : Structure and Properties*, p. 24 ; Butterworths, 1976.

DISTRIBUTION

Oak Ridge National Laboratory

1. Childs, K. W.
2. Kirkpatrick, J. R.
3. Ludtka, G. M.
4. Spooner, S.

Oak Ridge Y-12 National Security Complex

5. Baker, M. L.
6. Bird, E. L.
7. Bonner, R. B. (2)
9. Bridges, R. L.
13. Bullock, J. S. (4)
14. Carpenter, D. A.
15. Lamberti, V. E.
16. McKenzie, P. E.
17. O'Hara, M. J.
18. Y-12 Central Files (RC)

Los Almos National Laboratory

19. Hanrahan, R.